Figure S1

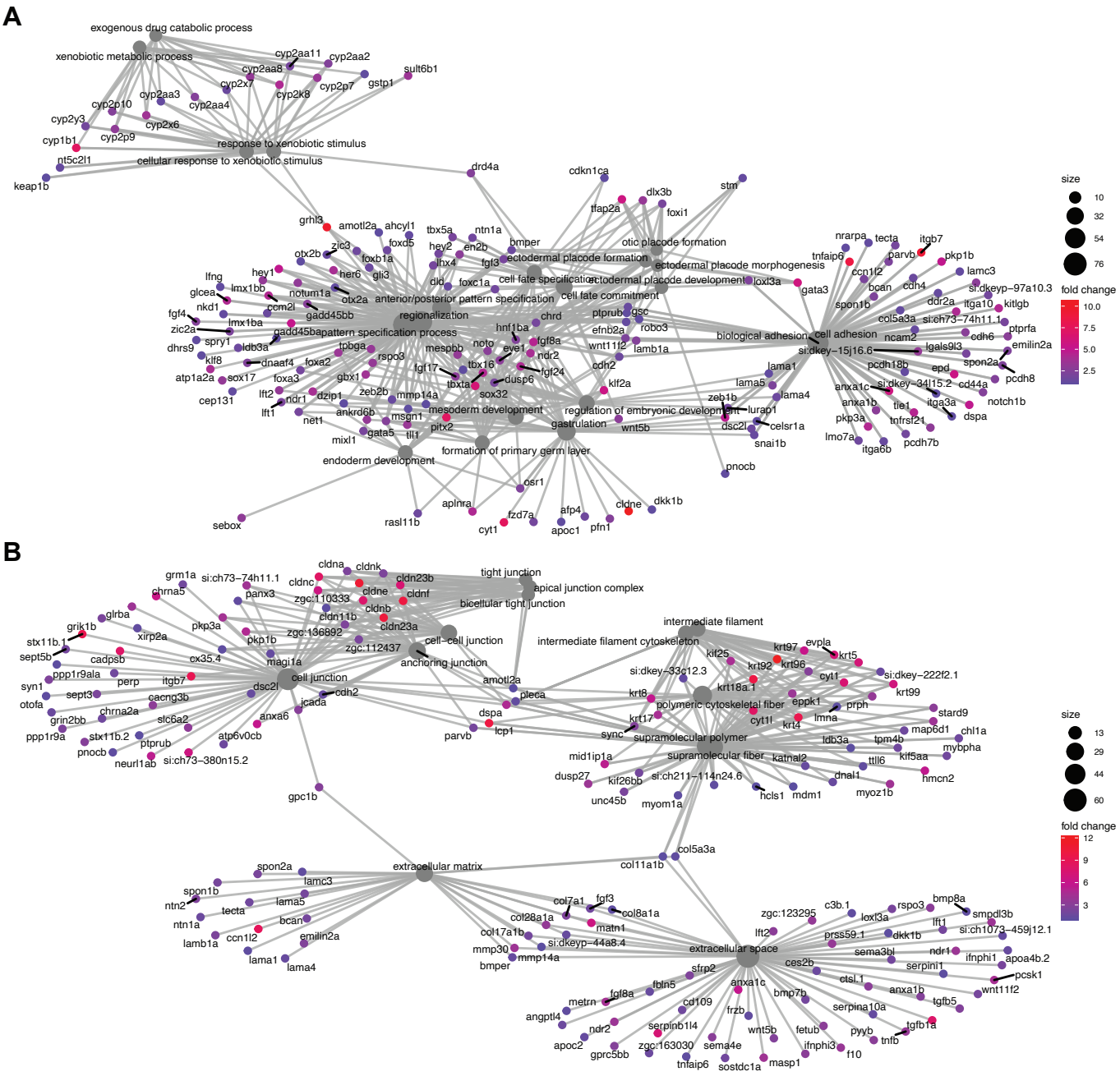
A
exogenous drug catabolic process
xenobiotic metabolic process
cyp2aa11
cyp2aa2
cyp2aa8
sult6b1
cyp2x7
cyp2p7
gstp1
cyp2k8
cyp2p10
cyp2aa3
cyp2aa4
cyp2y3
cyp2x6
cyp1b1
cyp2p9
response to xenobiotic stimulus
nt5c2l1
cellular response to xenobiotic stimulus
keap1b
drd4a
cdkn1ca
dlx3b
stm
tfap2a
foxi1
otic placode formation
ectodermal placode formation
ectodermal placode morphogenesis
ectodermal placode development
loxl3a
gata3
grhl3
amotl2a
ahcyl1
tbx5a
ntn1a
bmper
en2b
hey2
foxd5
otx2b
zic3
foxb1a
lhx4
fgf3
dld
foxc1a
cell fate specification
cell fate commitment
anterior/posterior pattern specification
regionalization
pattern specification process
lfng
hey1
her6
gli3
lmx1bb
notum1a
otx2a
glcea
nkd1
ccm2l
gadd45bb
fgf4
lmx1ba
gadd45ba
zic2a
spry1
dhrs9
ldb3a
klf8
dnaaf4
foxa2
atp1a2a
sox17
foxa3
cep131
lft2
ndr1
lft1
dzip1
net1
zeb2b
ankrd6b
mmp14a
msgn1
gata5
tll1
mixl1
endoderm development
tpbga
rspo3
mespbb
noto
eve1
hnf1ba
fgf8a
ndr2
tbx16
fgf17
fgf24
tbxta
dusp6
sox32
chrd
ptprub
gsc
efnb2a
robo3
wnt11f2
lamb1a
cdh2
klf2
mesoderm development
regulation of embryonic development
gastrulation
wnt5b
pitx2
formation of primary germ layer
osr1
aplnra
rasl11b
fzd7a
afp4
cldne
dkk1b
cyt1
apoc1
pfn1
sebox
pnocb
biological adhesion
cell adhesion
si:dkey-15j16.6
lama1
lama5
lama4
zeb1b
lurap1
dsc2l
celsr1a
snai1b
nrarpa
tecta
itgb7
tnfaip6
parvb
pkp1b
ccn1l2
lamc3
bcan
cdh4
si:dkeyp-97a10.3
spon1b
ddr2a
itga10
kitlgb
col5a3a
si:ch73-74h11.1
ptprfa
ncam2
cdh6
lgals9l3
emilin2a
pcdh18b
epd
spon2a
pcdh8
anxa1c
si:dkey-34l15.2
cd44a
anxa1b
tie1
itga3a
notch1b
pkp3a
tnfrsf21
dspa
lmo7a
itga6b
pcdh7b
size
10
32
54
76
fold change
10.0
7.5
5.0
2.5
B
cldna
cldnk
cldn23b
tight junction
grm1a
si:ch73-74h11.1
cldnc
zgc:110333
cldne
cldnf
apical junction complex
chrna5
panx3
cldnb
bicellular tight junction
glrba
cldn11b
cldn23a
grik1b
pkp3a
zgc:136892
cell-cell junction
stx11b.1
xirp2a
pkp1b
zgc:112437
anchoring junction
sept5b
cadpsb
cx35.4
magi1a
ppp1r9ala
perp
itgb7
cell junction
amotl2a
syn1
dsc2l
cdh2
sept3
cacng3b
pleca
otofa
jcada
chrna2a
dspa
grin2bb
slc6a2
anxa6
lcp1
parvb
ppp1r9a
stx11b.2
atp6v0cb
ptprub
pnocb
si:ch73-380n15.2
neurl1ab
gpc1b
intermediate filament
intermediate filament cytoskeleton
krt97
evpla
kif25
krt5
krt92
krt96
si:dkey-33c12.3
cyt1
si:dkey-222f2.1
krt18a.1
krt99
krt8
polymeric cytoskeletal fiber
eppk1
prph
stard9
cyt1l
krt17
lmna
krt4
map6d1
chl1a
sync
supramolecular polymer
ldb3a
tpm4b
mybpha
mid1ip1a
supramolecular fiber
katnal2
ttll6
klf5aa
dusp27
kif26bb
si:ch211-114n24.6
dnal1
hmcn2
unc45b
myom1a
hcls1
mdm1
myoz1b
col5a3a
col11a1b
extracellular matrix
spon2a
lamc3
spon1b
ntn2
lama5
tecta
ntn1a
bcan
lamb1a
ccn1l2
emilin2a
lama1
lama4
col7a1
fgf3
col8a1a
col28a1a
matn1
col17a1b
si:dkeyp-44a8.4
mmp30
mmp14a
bmper
extracellular space
zgc:123295
c3b.1
rspo3
bmp8a
loxl3a
smpdl3b
lft2
prss59.1
dkk1b
lft1
si:ch1073-459j12.1
sema3bl
ndr1
ifnphi1
apoa4b.2
ces2b
serpini1
pcsk1
sfrp2
ctsl.1
anxa1b
wnt11f2
anxa1c
bmp7b
tgfb5
fbln5
fgf8a
metrn
cd109
serpina10a
angptl4
frzb
tgfb1a
ndr2
serpinb1l4
wnt5b
fetub
pyyb
tnfb
apoc2
zgc:163030
sema4e
ifnphi3
f10
gprc5bb
tnfaip6
sostdc1a
masp1
size
13
29
44
60
fold change
12
9
6
3

Figure S1. Gene ontology (GO) gene-concept network analysis of RNA-seq data. (A) *irf6*-/- embryos have perturbations in biological processes such as cell adhesion, gastrulation, mesoderm, ectoderm and endoderm development, and response to xenobiotic stimulus. (B) *irf6*-/- embryos also have perturbations of various cellular compartments including cell junctions, cytoskeletal elements and extracellular space. Grey nodes show GO terms, colored nodes show individual genes from the RNA-seq dataset, and edges connect genes to one or more associated GO terms. Colored nodes show relative enrichment (measured by fold-change) of genes in wild type samples relative to *irf6-/-* embryos. Maps were generated using the enrichplot package in R.

Development • Supplementary information

Figure S2

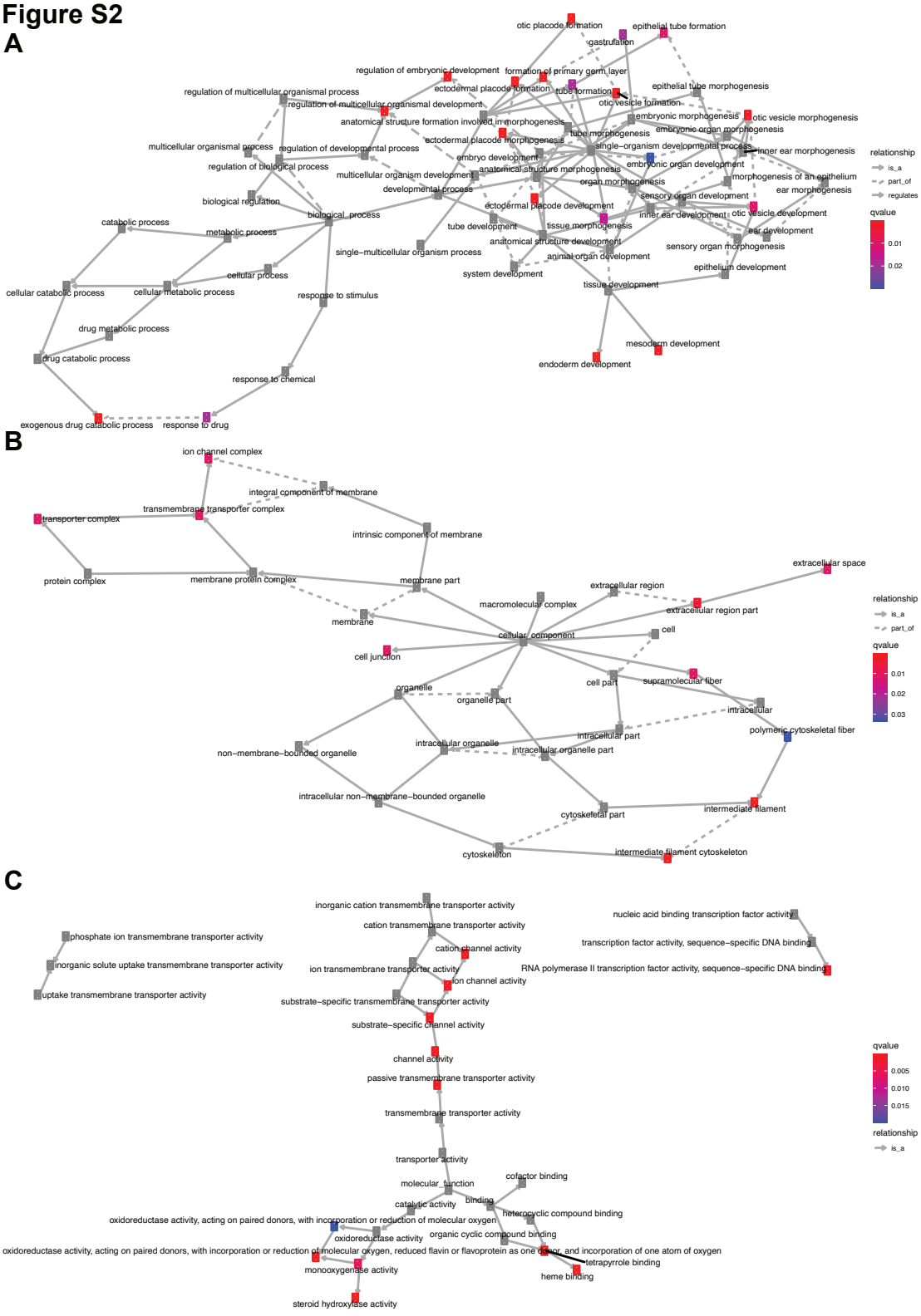
A
otic placode formation
epithelial tube formation
gastrulation
regulation of embryonic development
formation of primary germ layer
ectodermal placode formation
tube formation
epithelial tube morphogenesis
regulation of multicellular organismal process
regulation of multicellular organismal development
otic vesicle formation
anatomical structure formation involved in morphogenesis
embryonic morphogenesis
otic vesicle morphogenesis
ectodermal placode morphogenesis
tube morphogenesis
embryonic organ morphogenesis
multicellular organismal process
regulation of developmental process
single−organism developmental process
inner ear morphogenesis
embryo development
regulation of biological process
anatomical structure morphogenesis
embryonic organ development
multicellular organism development
organ morphogenesis
morphogenesis of an epithelium
developmental process
sensory organ development
ear morphogenesis
biological regulation
ectodermal placode development
inner ear development
otic vesicle development
biological_process
catabolic process
tube development
tissue morphogenesis
ear development
metabolic process
anatomical structure development
sensory organ morphogenesis
single−multicellular organism process
animal organ development
cellular process
system development
epithelium development
tissue development
cellular catabolic process
cellular metabolic process
response to stimulus
drug metabolic process
mesoderm development
drug catabolic process
endoderm development
response to chemical
exogenous drug catabolic process
response to drug
relationship
is_a
part_of
regulates
qvalue
0.01
0.02
B
ion channel complex
integral component of membrane
transmembrane transporter complex
transporter complex
intrinsic component of membrane
extracellular space
protein complex
membrane protein complex
membrane part
extracellular region
macromolecular complex
extracellular region part
membrane
cell
cellular_component
cell junction
cell part
supramolecular fiber
organelle
organelle part
intracellular
polymeric cytoskeletal fiber
intracellular part
intracellular organelle
non−membrane−bounded organelle
intracellular organelle part
intracellular non−membrane−bounded organelle
cytoskeletal part
intermediate filament
cytoskeleton
intermediate filament cytoskeleton
relationship
is_a
part_of
qvalue
0.01
0.02
0.03
C
inorganic cation transmembrane transporter activity
nucleic acid binding transcription factor activity
cation transmembrane transporter activity
phosphate ion transmembrane transporter activity
transcription factor activity, sequence−specific DNA binding
cation channel activity
inorganic solute uptake transmembrane transporter activity
ion transmembrane transporter activity
RNA polymerase II transcription factor activity, sequence−specific DNA binding
ion channel activity
uptake transmembrane transporter activity
substrate−specific transmembrane transporter activity
substrate−specific channel activity
channel activity
passive transmembrane transporter activity
transmembrane transporter activity
transporter activity
cofactor binding
molecular_function
catalytic activity
binding
oxidoreductase activity, acting on paired donors, with incorporation or reduction of molecular oxygen
heterocyclic compound binding
oxidoreductase activity
organic cyclic compound binding
oxidoreductase activity, acting on paired donors, with incorporation or reduction of molecular oxygen, reduced flavin or flavoprotein as one donor, and incorporation of one atom of oxygen
tetrapyrrole binding
monooxygenase activity
heme binding
steroid hydroxylase activity
qvalue
0.005
0.010
0.015
relationship
is_a

Figure S2. GO Enrichment analysis of the wt vs. mz-*irf6*-/- RNA-seq dataset.

Nodes show GO terms associated with enriched genes in the dataset. Edges and arrows show previously annotated relationships between GO terms. Developmental processes such as ectodermal development and otic placode formation are enriched in the analysis, which involve the recruitment of neural crest cell progenitors also involved in palate development. Color represents q-value, with red having a lower q-value and blue having a higher q-value. Q-values were computed using FDR with the Benjamini-Hochberg correction. Data were visualized using the enrichGO and goplot packages in R.

Development • Supplementary information

Figure S3

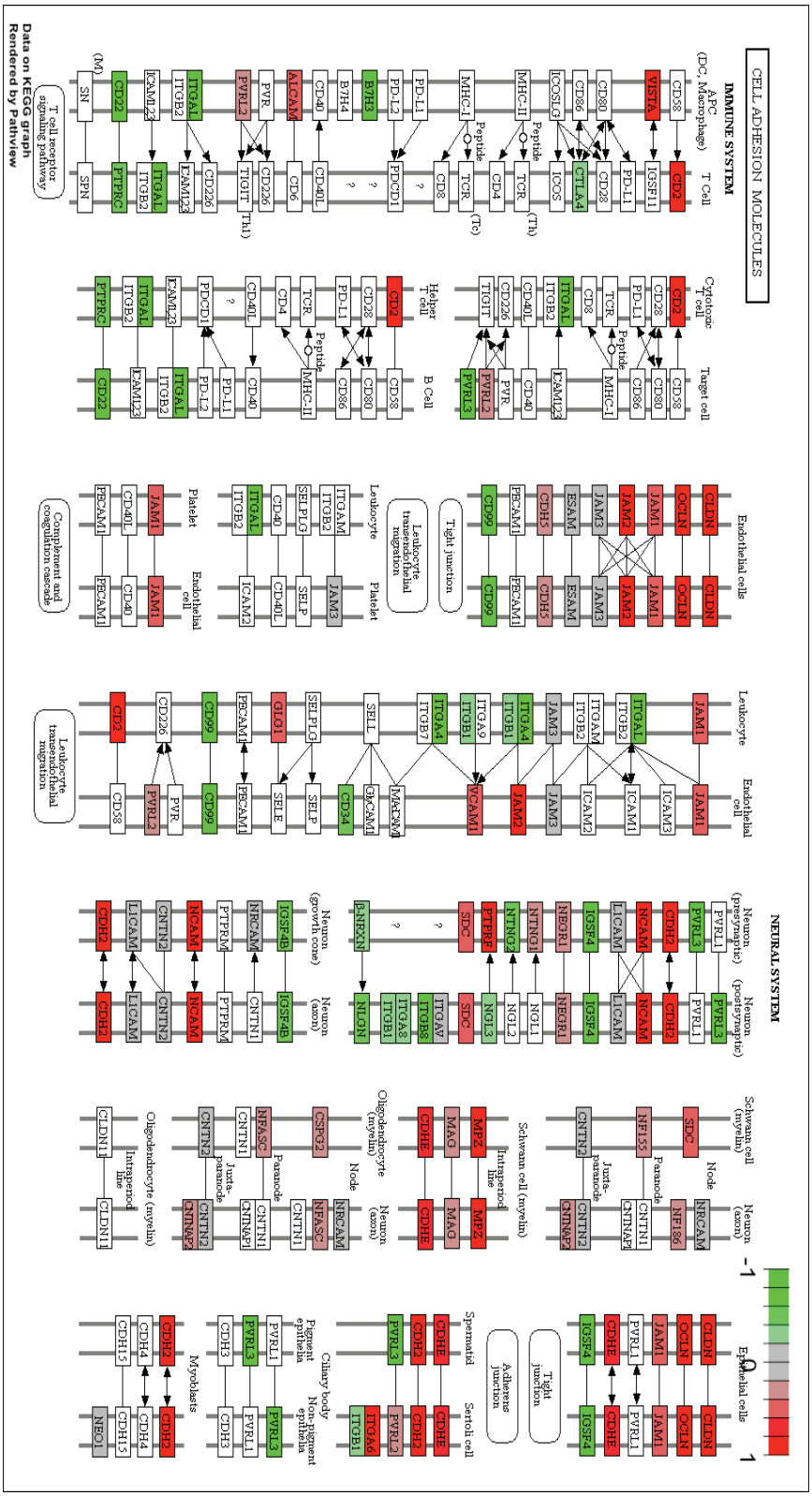

Development • Supplementary information

Figure S3. KEGG Graph of Cell Adhesion Molecules. KEGG pathway analysis that maps enriched genes in our dataset to a database containing cellular pathway information. Colored nodes show increased expression of genes in red and decreased expression in green for wild type fish compared to control. Many cell-adhesion molecular interactions are disrupted in the *irf6*-/- embryos. Data were generated using the enrichKEGG and pathview packages in R.

Development • Supplementary information

Figure S4

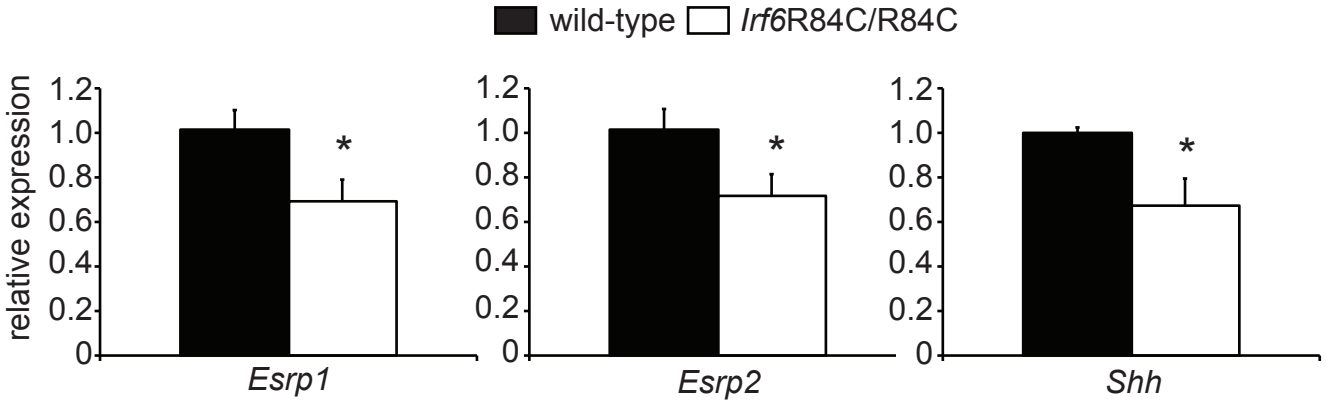

Figure S4. Decreased expression of *Esrp1* and *Esrp2* in *Irf6*R84C mutant mouse embryos. *Irf6*$^{R84C/WT}$ mice were intercrossed, and embryos were collected at E11.5. Embryos were individually genotyped and heads of *Irf6*$^{WT/WT}$ and *Irf6*$^{R54C/R84C}$ embryos were utilized for RNA isolation and RT-qPCR. Expression of *Esrp1*, *Esrp2* and *Shh* were significantly decreased in the *Irf6*$^{R54C/R84C}$ embryos relative to wild type. Expression levels were normalized to *TBP* expression. n=5. Students t-test, $p<0.05$.

Development • Supplementary information

Figure S5

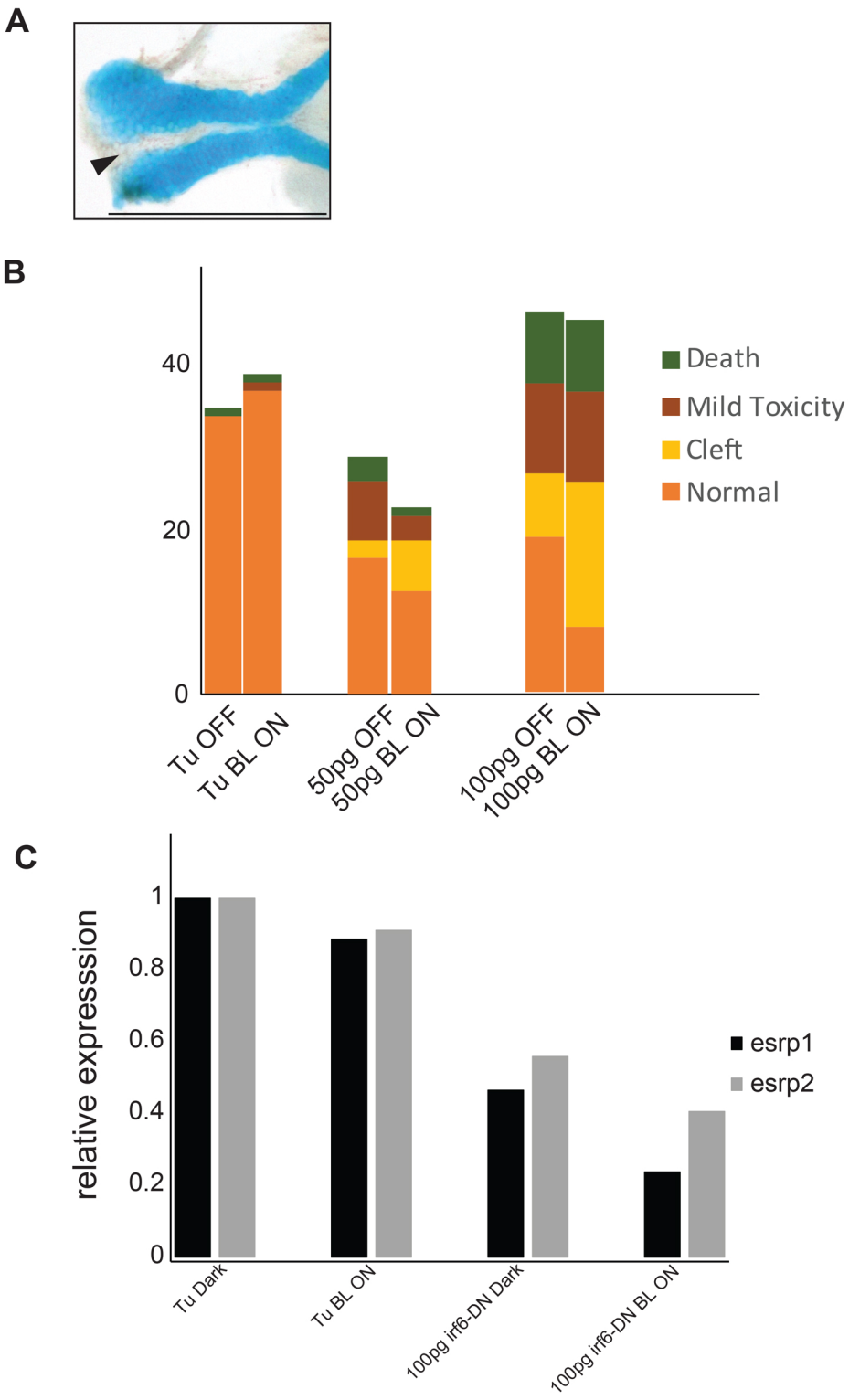

Development • Supplementary information

Figure S5. Optogenetic disruption of *irf6*. (A) Cleft ANC phenotype observed in *irf6*-DN embryos exposed to blue light at 10 hpf. (B) Distribution of observed phenotype in wild type (uninjected) vs. *irf6*-DN injected embryos at 50pg/50pg or 100pg/100pg doses of poly-A tailed EL222-VP16 mRNA and (C120)-*irf6*-DN plasmid grown in the dark or exposed to blue light at 10 hpf. Bar chart height represents absolute number of embryos. (C) qPCR gene expression analysis for *esrp1* and *esrp2*, showing approximately two-fold and five-fold reduction in *esrp1* expression in embryos injected with the optogenetic *irf6-DN* system grown in the dark, or under blue light, respectively. *esrp2* follows a similar trend. Scale bars: 150um.

Development • Supplementary information

Figure S6

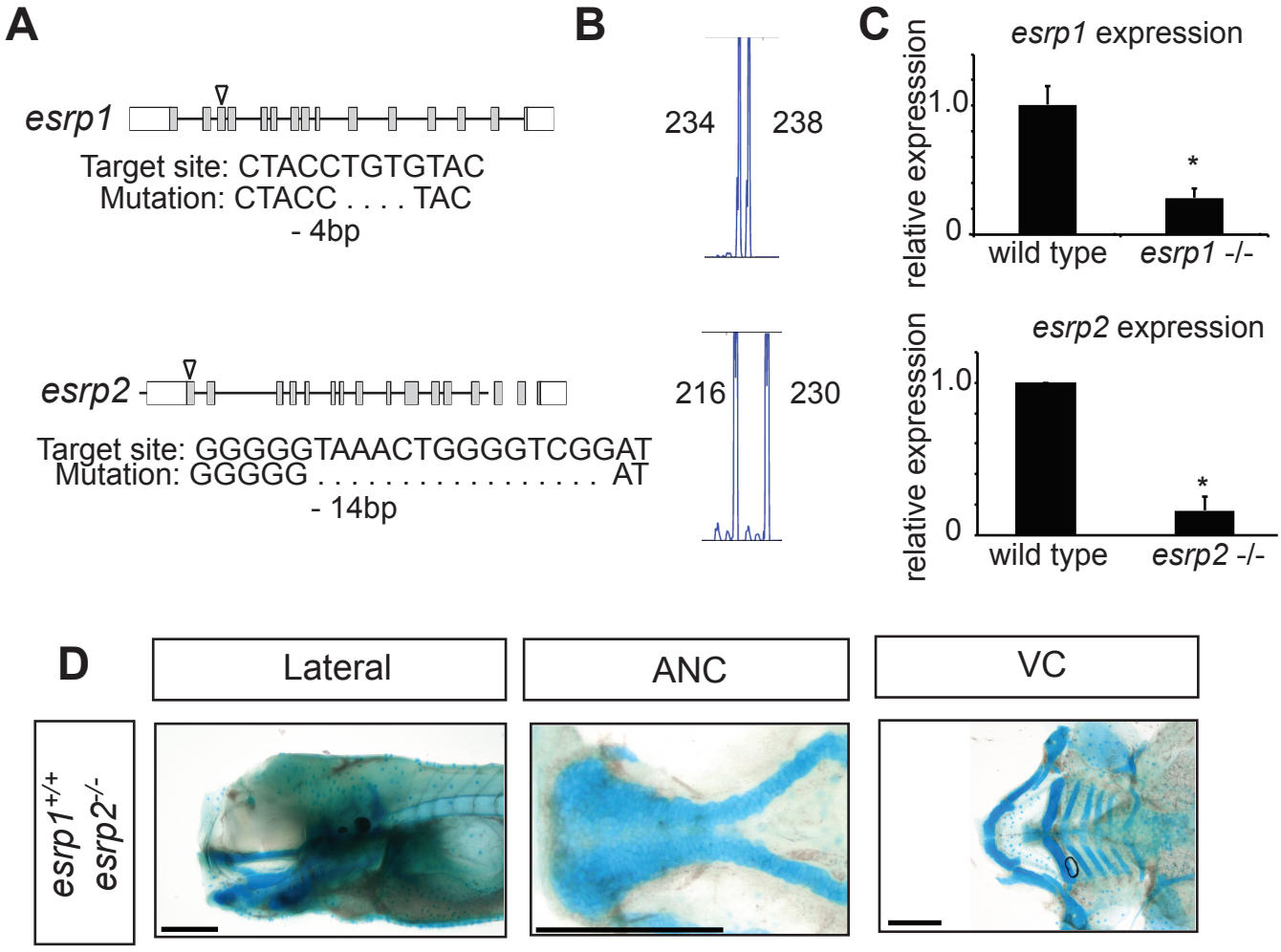

Figure S6. Generation of *esrp1* and *esrp2* CRISPR/Cas9 gene disruption in zebrafish. (A) Schematic representations of *esrp1* and *esrp2* exons, positions of target site (arrow), and sequences of mutations. (B) Micro-satellite results of genotyping PCR showing a size shift consistent with the observed mutation. (C) Expression of the CRISPR/Cas9 targeted gene is decreased relative to wild type, as measured by qPCR. n=3,4. $p<0.01$ (D) *esrp1*$^{+/+}$; *esrp2*$^{-/-}$ fish embryos at 4dpf exhibit normal craniofacial development of the anterior neurocranium and ventral cartilages. Scale bars: 200um.

Development • Supplementary information

Figure S8

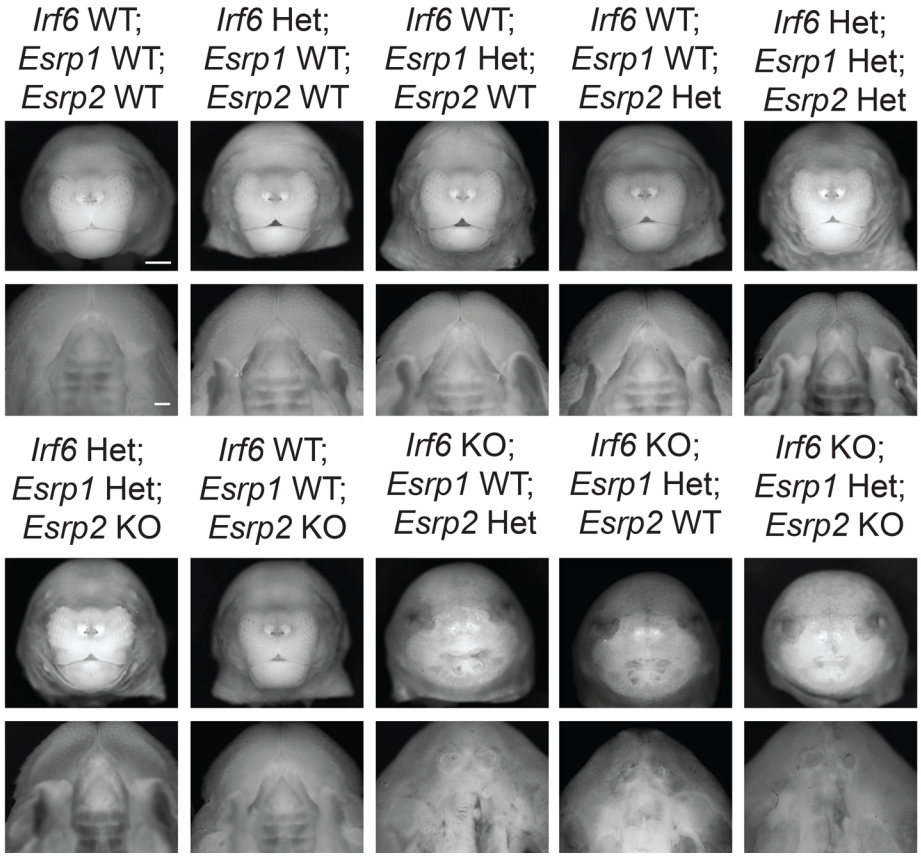

Figure S7. Representative images of *Irf6*$^{R84C/WT}$; *Esrp1*$^{+/-}$; *Esrp2*$^{+/-}$ triple heterozygote in-crosses. Mice compound heterozygous for *Irf6*^{R84C}, *Esrp1* and *Esrp2* were generated by breeding *Irf6*$^{R84C/+}$ with *Esrp1*$^{+/-}$; *Esrp2*$^{-/-}$ mice. The triple heterozygotes were then inter-crossed and embryos were collected at E18.5. Representative frontal and oral images of embryos displaying no craniofacial phenotype in single heterozygotes, triple heterozygotes or *Irf6*$^{R84C/+}$; *Esrp1*$^{+/-}$; *Esrp2*$^{-/-}$. Further, Esrp1/2 alleles did not appear to modify *Irf6*$^{R84C/R84C}$ phenotype, however epithelial adhesions hampered a thorough observation. Scale bar: 100 μm.

Table S1. *Irf6, Esrp1* and *Esrp2* genotypes interact to produce non-Mendelian embryo ratios.

Click here to Download Table S1

Development • Supplementary information

Table S2. Irf6, Esrp1 and Esrp2 genotypes interact to produce non-Mendelian embryo ratios

Irf6	*Esrp1*	*Esrp2*	probability	Expected	Observed
WT	WT	WT	1/64	1.2	3
WT	WT	Het	1/32	2.5	4
WT	WT	KO	1/64	1.2	1
WT	Het	WT	1/32	2.5	2
WT	Het	Het	1/16	4.9	3
WT	Het	KO	1/32	2.5	4
WT	KO	WT	1/64	1.2	0
WT	KO	Het	1/32	2.5	1
WT	KO	KO	1/64	1.2	1
Het	WT	WT	1/32	2.5	5
Het	WT	Het	1/16	4.9	4
Het	WT	KO	1/32	2.5	3
Het	Het	WT	1/16	4.9	10
Het	Het	Het	1/8	9.9	8
Het	Het	KO	1/16	4.9	2
Het	KO	WT	1/32	2.5	2
Het	KO	Het	1/16	4.9	6
Het	KO	KO	1/32	2.5	3
KO	WT	WT	1/64	1.2	1
KO	WT	Het	1/32	2.5	2
KO	WT	KO	1/64	1.2	0
KO	Het	WT	1/32	2.5	5
KO	Het	Het	1/16	4.9	4
KO	Het	KO	1/32	2.5	5
KO	KO	WT	1/64	1.2	0
KO	KO	Het	1/32	2.5	0
KO	KO	KO	1/64	1.2	0

Irf6R84C/WT; *Esrp1*+/-; *Esrp2*+/- triple heterozygous mice were in-crossed and embryos were collected between E12.5 and E21. Table 1 is a subset of expected number of embryos based on Mendelian genetics versus the observed number of viable embryos. The *Irf6R84C/R84C*; *Esrp1*-/- genotype appears to be lethal prior to E12.5 as approximately 5 embryos were expected but zero embryos were observed. A total of 79 embryos were collected from 9 different litters.

Development • Supplementary information